

无机化学学报

2019年

第35卷

第5期

目次

综述

铁基催化剂用于氨选择性催化还原氮氧化物研究进展

.....张洪亮 龙红明 李家新 董林(753)

论文

有双重固硫作用的 PEDOT 包覆 MnO_2 纳米管阴极用于高性能的锂硫电池(英文)

.....葛优 潘沛锋 彭霞 刘瑞卿
朱红丽 冯晓苗 沈清明 黄镇东 马延文(769)

细胞内不同形态 Gd 基 MRI 造影剂的 T_1/T_2 弛豫性能及造影效果

.....孙兴丽 张艳辉 赵敏敏 谭波 张海禄 邓宗武(780)

一个三羧酸配体构筑的钷金属-有机框架材料及对小分子溶剂的荧光识别

.....林鸿 吕灵芝 冯云龙(787)

一锅法制备 $\text{Co}_3\text{O}_4/\text{g-C}_3\text{N}_4$ 复合光催化剂及其光催化性能

.....段丽颖 路姗姗 段芳 陈明清(793)

$\text{Na}_2\text{MoO}_4 \cdot 2\text{H}_2\text{O}$ 晶体及其熔体结构的温致拉曼光谱

.....丁雅妮 尤静林 王敏 Lu Liming 王建 曹培明 徐琰东(803)

稀土掺杂钒酸镧微球的制备及其光催化降解抗生素

.....王晓丽 张琳萍 周培文 钟毅
徐红 隋晓锋 冯雪凌 陈支泽 王碧佳 毛志平(812)

乙醛低温绿色合成:焦磷酸锆催化乳酸脱羧反应

.....唐聪明 张瑜 李新利 谭平华 邹伟欣 董林 庞均 张菊(819)

氨基化硅藻基 As(V)印迹复合材料的制备与性能

.....梁效铭 钟溢健 马丽丽 李聪 杨勤桃 陈南春 解庆林(828)

由醋酸根桥连构筑的零维六核镉(II)格子型配合物和一维锌(II)配位聚合物的合成、晶体结构及荧光性质

.....鲁圣楠 吴文士 石凤湘 全志龙(837)

两性表面活性剂插层 GO-LDH 的制备和性能

.....刘浩翔 刘昌霞 陈璐佳 张晓光(844)

由 2-(4'-羧基苯基)咪唑-4,5-二羧酸构筑的过渡金属配位聚合物的合成、结构及性质

.....鲁雅 管全银 张敏芝 赵国良(855)

基于陶瓷/聚合物的准固态复合电解质的制备及电化学性能

.....孙秋实 朱崇佳 谢健 曹高劲
赵新兵 郑东 金源 王康彦 郭永斌 屠芳芳(865)

- HgI₂-HI-H₂O 溶液中静电场诱导的 α -碘化汞晶体生长
许 岗 张 改 杨丛笑 陈 静 侯雁楠 李俊英 谷 智(871)
- 硅化钴的简单固相合成与磁学性能(英文)
朱炳龙 陆铃鲸 戴伟城 张赐阳 方礼炜 王 迪 王佳健(876)
- 有机相化学镀铝法制备 Al/石墨烯复合材料粉末(英文)
段 政 徐明英 高建峰 郝 敏 刘 艳 马 洁 白培康(881)
- 羟基磷灰石负载放射性 ¹⁸F 作为分子影像纳米探针在生物学中的应用(英文)
吴 睿 卢久富 宋 娟 刘存芳 张 强 田光辉(891)
- 五个吡嗪缩氨基硫脲过渡金属配合物的合成、结构和荧光性质(英文)
高亮亮 黄山秀 康瑞芳 代耿耿 吴伟娜 王 元 陈 忠(901)
- 五配位单核钴配合物的单晶结构和磁性能(英文)
张翠娟 Sukhen Bala 倪兆平 童明良(910)
- Cr³⁺和 Ni²⁺复合掺杂的尖晶石氧化物用于提高钴孔热电池放电性能(英文)
宋恒旭 牛永强 赵宇宏 连冬晓 任敬霞 张妍妍 侯 华(915)
- 在纯水体系和活细胞中高选择检测 Fe³⁺的香豆素荧光探针(英文)
刘琪梦 汪 欢 郭昊冉 郭 媛(923)
- 一种 2-甲基-3-羟基喹啉-4-甲酸单核铜(II)配合物的合成、晶体结构、理论计算与性质(英文)
方小牛 李 佳 易绣光 易志强 陈家怡 李永绣(930)

CHINESE JOURNAL OF INORGANIC CHEMISTRY

Vol.35

No.5

May 2019

CONTENTS

Cover



Dual-Confined Sulfur Cathodes Encapsulated in MnO_2 Nanotubes and Wrapped with PEDOT for High-Performance Lithium-Sulfur Batteries (English)

GE You, PAN Pei-Feng, PENG Xia, LIU Rui-Qing, ZHU Hong-Li, FENG Xiao-Miao, SHEN Qing-Ming, HUANG Zhen-Dong, MA Yan-Wen

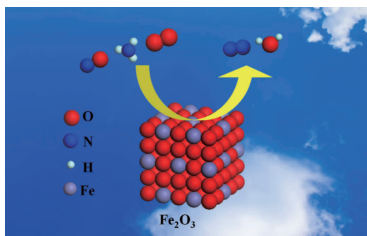
DOI:10.11862/CJIC.2019.093

Chinese J. Inorg. Chem., 2019,35(5):769-779

Reviews

Research Progress in Iron-Based Catalysts for the Selective Catalytic Reduction of NO_x by NH_3

ZHANG Hong-Liang, LONG Hong-Ming, LI Jia-Xin, DONG Lin



Low-temperature NH_3 -SCR has attracted considerable attention owing to the vast demand in industrial furnaces and its energy-conserving feature. This review summarizes the recent advances in the application of iron-based catalysts for the selective catalytic reduction of NO_x by NH_3 .

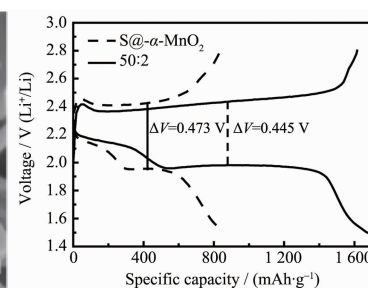
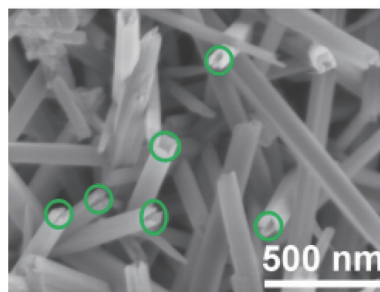
DOI:10.11862/CJIC.2019.099

Chinese J. Inorg. Chem., 2019,35(5):753-768

Articles

Dual-Confined Sulfur Cathodes Encapsulated in MnO_2 Nanotubes and Wrapped with PEDOT for High-Performance Lithium-Sulfur Batteries (English)

GE You, PAN Pei-Feng, PENG Xia, LIU Rui-Qing, ZHU Hong-Li, FENG Xiao-Miao, SHEN Qing-Ming, HUANG Zhen-Dong, MA Yan-Wen



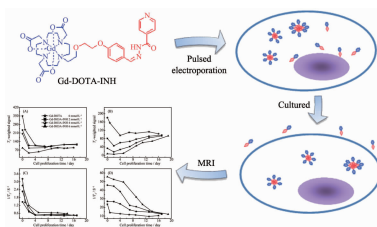
Urchin-like α - MnO_2 -PEDOT nanotubes were fabricated through a facile template-free hydrothermal self-assembly in situ polymerization as sulfur host material for high performance lithium-sulfur batteries.

DOI:10.11862/CJIC.2019.093

Chinese J. Inorg. Chem., 2019,35(5):769-779

T_1/T_2 Relaxation and MRI Contrast Effect of Gd Agent in Different Intracellular Forms

SUN Xing-Li, ZHANG Yan-Hui, ZHAO Min-Min, TAN Bo, ZHANG Hai-Lu, DENG Zong-Wu



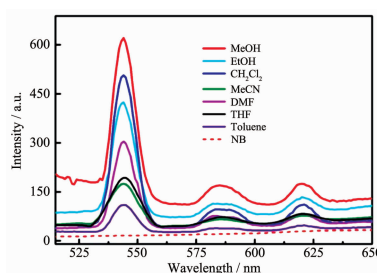
Gd-DO3A-INH as MRI contrast agent was introduced into hMSCs in two different forms: free Gd-DO3A-INH and Gd-DO3A-INH nanocluster. Cellular MRI discloses that free Gd-DO3A-INH is in favor of acceleration of T_1 relaxation and exhibits fast exocytosis, Gd-DO3A-INH nanocluster is in favor of acceleration of T_2 relaxation and exhibits promoted cell retention time, yielding a fast recovery of T_1 -weighted contrast and a delayed recovery of T_2 -weighted contrast during cell proliferation.

DOI:10.11862/CJIC.2019.100

Chinese J. Inorg. Chem., **2019**,**35**(5):780-786

One Terbium-Metal Organic Framework Based on a Tricarboxylate Ligand for Sensing of Small Molecule Solvents

LIN Hong, LÜ Ling-Zhi, FENG Yun-Long



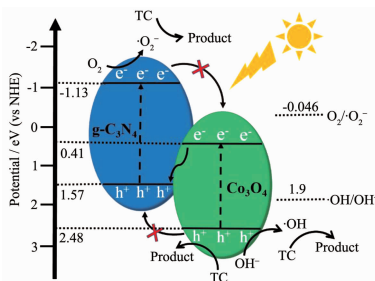
Tb-MOF exhibits highly selective and sensitive sensing for small organic molecules. The significant quenching in nitrobenzene indicates that it is potential luminescent sensing material for nitro explosives.

DOI:10.11862/CJIC.2019.103

Chinese J. Inorg. Chem., **2019**,**35**(5):787-792

Preparation and Photocatalytic Activity of $\text{Co}_3\text{O}_4/\text{g-C}_3\text{N}_4$ Composite Photocatalysts via One-Pot Synthesis

DUAN Li-Ying, LU Shan-Shan, DUAN Fang, CHEN Ming-Qing



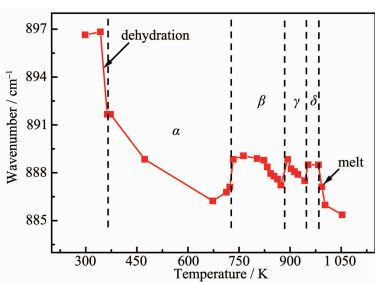
$\text{Co}_3\text{O}_4/\text{g-C}_3\text{N}_4$ composite photocatalysts with porous structure and high specific surface areas were prepared through a one-pot process. The formed $\text{Co}_3\text{O}_4/\text{g-C}_3\text{N}_4$ heterojunctions can effectively transfer the photon-generated carriers and decrease the recombination rate of electrons and holes, thus the photocatalytic activity can be effectively improved.

DOI:10.11862/CJIC.2019.087

Chinese J. Inorg. Chem., **2019**,**35**(5):793-802

Temperature Dependent Raman Spectra of $\text{Na}_2\text{MoO}_4 \cdot 2\text{H}_2\text{O}$ Crystal and Its Melt Structure

DING Ya-Ni, YOU Jing-Lin, WANG Min, LU Liming, WANG Jian, CAO Pei-Ming, XU Yan-Dong



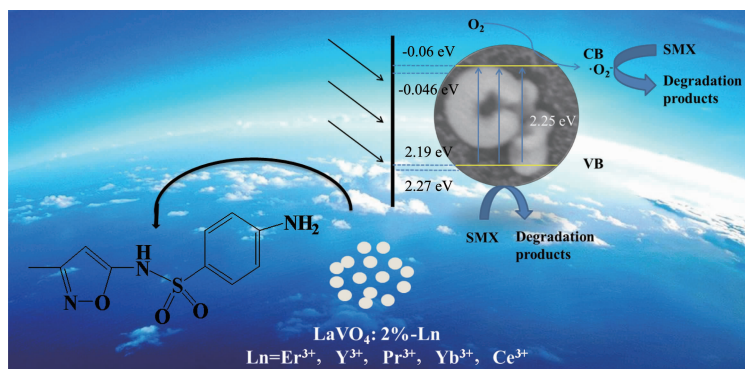
The $\text{Na}_2\text{MoO}_4 \cdot 2\text{H}_2\text{O}$ crystal undergoes the process of dehydration, phase transformation and melting while being heated. Temperature has significant effect on the wavenumber of Mo-O symmetric stretching vibrational mode of the isolated $[\text{MoO}_4]^{2-}$. Variations in the average bond length of Mo-O bonds in $[\text{MoO}_4]^{2-}$ can be derived.

DOI:10.11862/CJIC.2019.086

Chinese J. Inorg. Chem., **2019**,**35**(5):803-811

Preparation and Photocatalytic Degradation Property of Antibiotics of Rare Earth Doped Microspherical LaVO_4 Photocatalysts

WANG Xiao-Li, ZHANG Lin-Ping, ZHOU Pei-Wen, ZHONG Yi, XU Hong, SUI Xiao-Feng, FENG Xue-Ling, CHEN Zhi-Ze, WANG Bi-Jia, MAO Zhi-Ping



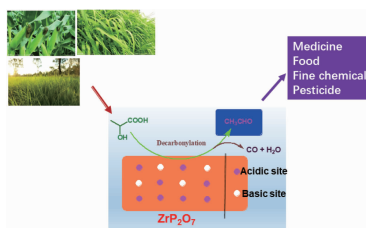
$\text{LaVO}_4:2\text{-Ln}$ ($\text{Ln}=\text{Er}^{3+}, \text{Y}^{3+}, \text{Pr}^{3+}, \text{Yb}^{3+}, \text{Ce}^{3+}$) photocatalyst produced $\cdot\text{O}_2^-$ and h^+ under light conditions to degrade antibiotic sulfamethoxazole (SMX).

DOI:10.11862/CJIC.2019.108

Chinese J. Inorg. Chem., **2019**,**35**(5):812-818

Green Synthesis of Acetaldehyde at Low Temperature: Decarbonylation of Lactic Acid Catalyzed by Zirconium Pyrophosphate

TANG Cong-Ming, ZHANG Yu, LI Xin-Li, TAN Ping-Hua, ZOU Wei-Xin, DONG Lin, PANG Jun, ZHANG Ju



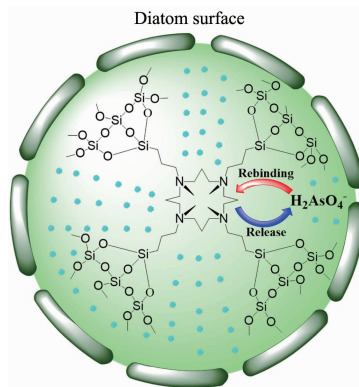
Zirconium pyrophosphate offered an excellent activity and durability for decarbonylation of lactic acid to acetaldehyde ascribing to moderate acidic sites and basic sites.

DOI:10.11862/CJIC.2019.109

Chinese J. Inorg. Chem., **2019**,**35**(5):819-827

Preparation and Properties of Aminated Diatom-Based As(V) Imprinted Composites

LIANG Xiao-Ming, ZHONG Yi-Jian, MA Li-Li, LI Cong, YANG Qin-Tao, CHEN Nan-Chun, XIE Qing-Lin



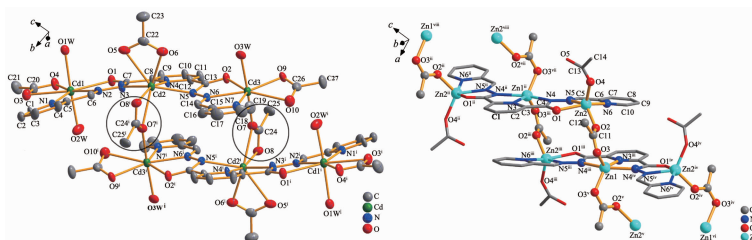
A diatom-based As(V) imprinted composite material was prepared by using diatom as a carrier, and the functional group amino group was grafted on the surface of the diatom by APS modification. An As(V) blot recognition site was formed on the surface of the diatom through the ECH cross-linking agent.

DOI:10.11862/CJIC.2019.102

Chinese J. Inorg. Chem., **2019**,**35**(5):828-836

Syntheses, Crystal Structures, and Fluorescence Properties of 0D Hexanuclear Cadmium(II) Grid Complex and 1D Zinc(II) Coordination Polymer Constructed by Acetate-Bridge

LU Sheng-Nan, WU Wen-Shi, SHI Feng-Xiang, QUAN Zhi-Long



Two new compounds have been successfully synthesized based on ligand Tppahz. It is obviously clear that the complex **1** is a grid structure, in triclinic, space group $P\bar{1}$. The complex **2** is a one-dimensional chain structure, belongs to monoclinic system, and space group $C2/c$.

DOI:10.11862/CJIC.2019.098

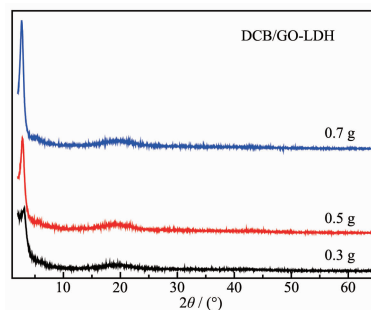
Chinese J. Inorg. Chem., **2019**,**35**(5):837-843

Preparation and Property of Zwitterionic Surfactants Intercalation into Graphene Oxide-Layered Double Hydroxide Hybrid

LIU Jie-Xiang, LIU Chang-Xia, CHEN Lu-Jia, ZHANG Xiao-Guang

DOI:10.11862/CJIC.2019.122

Chinese J. Inorg. Chem., **2019**,**35**(5):844-854



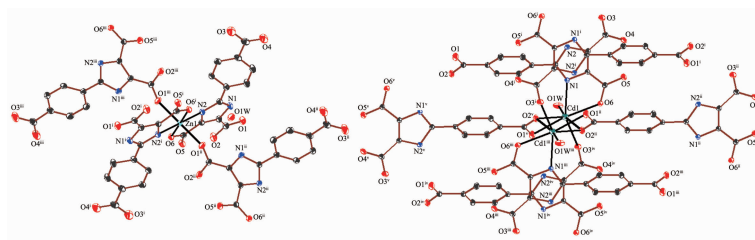
Dodecyl dimethyl carboxylbetaine (DCB) and dodecyl dimethyl sulfobetaine (DSB) were successfully intercalated into graphene oxide-layered double hydroxide (GO-LDH). The DCB/GO-LDH and DSB/GO-LDH prepared in water had the greater *d*-spacing values. CPF-DCB/GO-LDH displayed the slow release property.

Syntheses, Crystal Structures and Properties of Transition Metal Coordination Polymers Constructed by 2-(4'-Carboxyphenyl)-1*H*-imidazole-4,5-dicarboxylic Acid

LU Ya, GUAN Quan-Yin, ZHANG Min-Zhi, ZHAO Guo-Liang

DOI:10.11862/CJIC.2019.105

Chinese J. Inorg. Chem., **2019**,**35**(5):855-864



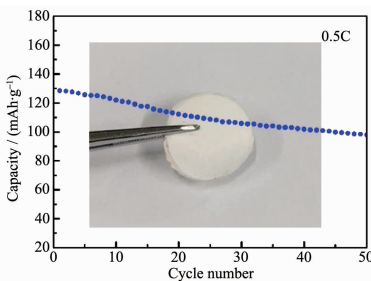
Four transition metal complexes of two series, $\{[M(H_3L)_2] \cdot 2H_2O\}_n$ ($M = Zn$ (**1**), Cd (**2**), Co (**3**)), $[Cd(H_2L)H_2O]_n$ (**4**) have been synthesized by solvothermal reaction from 2-(4'-carboxyphenyl)-1*H*-imidazole-4,5-dicarboxylic acid (H_4L) and characterized by IR, EA, TG, single crystal X-ray diffraction.

Preparation and Electrochemical Performance of Ceramic/Polymer-Based Quasi-Solid Composite Electrolyte

SUN Qiu-Shi, ZHU Chong-Jia, XIE Jian, CAO Gao-Shao, ZHAO Xin-Bing, ZHENG Dong, JIN Yuan, WANG Kang-Yan, GUO Yong-Bin, TU Fang-Fang

DOI:10.11862/CJIC.2019.097

Chinese J. Inorg. Chem., **2019**,**35**(5):865-870



A quasi-solid electrolyte obtained a high ionic conductivity of $1.3 \times 10^{-4} \text{ S} \cdot \text{cm}^{-1}$ at room temperature and the $\text{LiFePO}_4/\text{Li}$ cell with the electrolyte delivers a high discharge capacity of $128.4 \text{ mAh} \cdot \text{g}^{-1}$ and remained 80% of initial capacity after 50 cycles at 0.5C.

Growth of $\alpha\text{-HgI}_2$ Crystal in $\text{HgI}_2\text{-HI-H}_2\text{O}$ Solution by Applying Electric Field

XU Gang, ZHANG Gai, YANG Cong-Xiao, CHEN Jing, HOU Yan-Nan, LI Jun-Ying, GU Zhi

DOI:10.11862/CJIC.2019.095

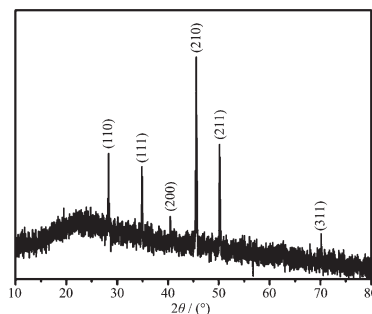
Chinese J. Inorg. Chem., **2019**,**35**(5):871-875



Morphology of $\alpha\text{-HgI}_2$ crystal in $\text{HgI}_2\text{-HI-H}_2\text{O}$ solution by applying electric field is an evidence that $[\text{HgI}_3]^-$ and $[\text{HgI}_4]^{2-}$ are also growth unit besides HgI_2 .

Facile Solid-State Synthesis and Magnetic Properties of Cobalt Monosilicide (English)

ZHU Bing-Long, LU Ling-Jing, DAI Wei-Cheng, ZHANG Ci-Yang, FANG Li-Wei, WANG Di, WANG Jia-Jian



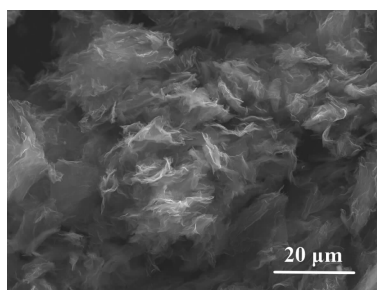
Cobalt monosilicide (CoSi) particles have been synthesized by utilizing cobalt oxide (Co_3O_4), silicon (Si) powder and metallic magnesium (Mg) as raw materials in a stainless steel autoclave.

DOI:10.11862/CJIC.2019.110

Chinese J. Inorg. Chem., **2019**,**35**(5):876-880

Synthesis of Al/graphene Composite Powder by Organic Phase Electroless Aluminum Plating (English)

DUAN Zheng, XU Ming-Ying, GAO Jian-Feng, HAO Min, LIU Yan, MA Jie, BAI Pei-Kang



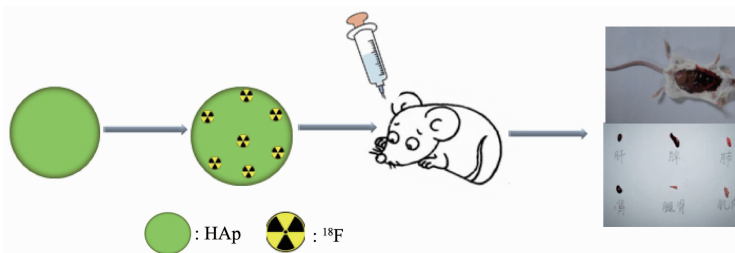
The Al/graphene composite powder was prepared in the organic phase by a simple method of electroless aluminum method. The effect of aluminum-plating is excellent, and aluminum can be well dispersed on the surface and interlayer of the graphene in the form of pure element.

DOI:10.11862/CJIC.2019.096

Chinese J. Inorg. Chem., **2019**,**35**(5):881-890

Hydroxyapatite Loaded Radiolabeled ^{18}F as Molecular Imaging Nanoprobes for Biomedical Application (English)

WU Rui, LU Jiu-Fu, SONG Juan, LIU Cun-Fang, ZHANG Qiang, TIAN Guang-Hui



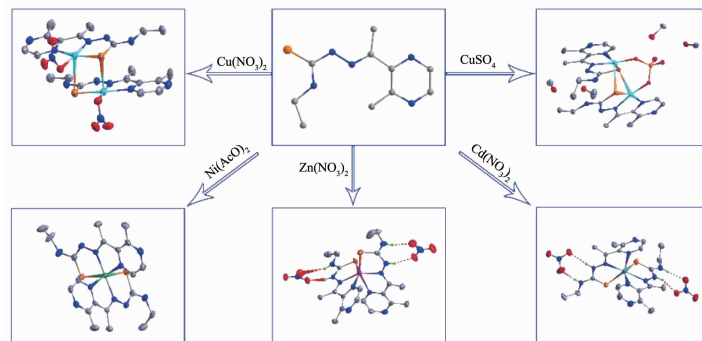
^{18}F was firmly doped in the synthesis process of HAP NPs in trace by strong chemical bond with the advantage of high load and prevention of radiation leakage. The designed PET probe was applied to the rats by tail vein to target to viscera organs.

DOI:10.11862/CJIC.2019.120

Chinese J. Inorg. Chem., **2019**,**35**(5):891-900

Crystal Structures and Fluorescence Properties of Five Transition Metal Complexes with Pyrazine Thiosemicarbazone (English)

GAO Liang-Liang, HUANG Shan-Xiu, KANG Rui-Fang, DAI Geng-Geng, WU Wei-Na, WANG Yuan, CHEN Zhong



Ni(II)/Zn(II)/Cd(II)/Cu(II) complexes based on a thiosemicarbazone ligand containing a pyrazine unit have been synthesized and characterized. The fluorescence spectra indicate that the interactions of the complexes with DNA are stronger than that of the ligand.

DOI:10.11862/CJIC.2019.065

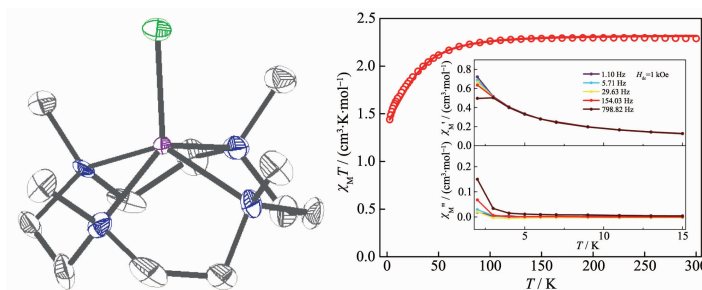
Chinese J. Inorg. Chem., **2019**,**35**(5):901-909

Crystal Structure and Magnetic Property of a Pentacoordinate Mononuclear Cobalt(II) Complex (English)

ZHANG Cui-Juan, Sukhen Bala, NI Zhao-Ping, TONG Ming-Liang

DOI:10.11862/CJIC.2019.104

Chinese J. Inorg. Chem., **2019**,**35**(5):910-914

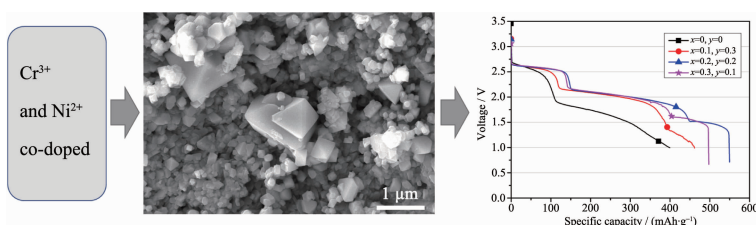


Cr^{3+} and Ni^{2+} Co-doped Spinel Oxide Cathode with Improved Capacity and Voltage Stability in Thermal Battery for Geothermal Borehole (English)

SONG Heng-Xu, NIU Yong-Qiang, ZHAO Yu-Hong, LIAN Dong-Xiao, REN Jing-Xia, ZHANG Yan-Yan, HOU Hua

DOI:10.11862/CJIC.2019.118

Chinese J. Inorg. Chem., **2019**,**35**(5):915-922



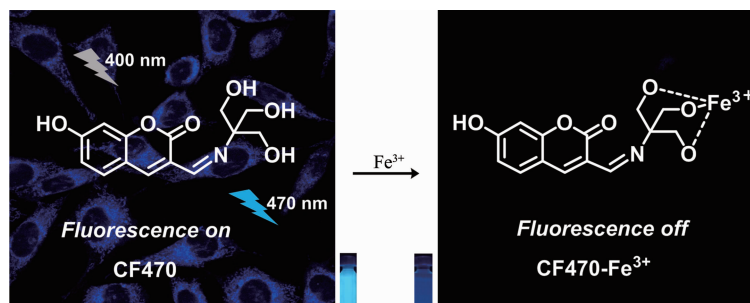
The $\text{LiCr}_x\text{Ni}_y\text{Mn}_{2-x-y}\text{O}_4/\text{LiNO}_3\text{-KNO}_3/\text{Li-Mg-B}$ battery system has a more significant improvement in discharge performance because the doping of chromium and nickel enhances the structural stability of spinel lithium manganate oxides.

A Highly Selective Coumarin-based Fluorescent Probe for Detecting Fe^{3+} in Pure Water Systems and Living Cells (English)

LIU Qi-Meng, WANG Huan, GUO Hao-Ran, GUO Yuan

DOI:10.11862/CJIC.2019.090

Chinese J. Inorg. Chem., **2019**,**35**(5):923-929

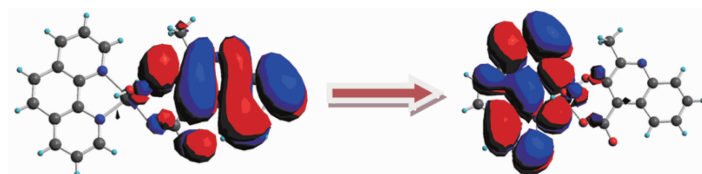


Synthesis, Crystal Structure, Theoretical Calculation and Properties of Cu(II) Complex with 3-Hydroxy-2-methylquinoline-4-carboxylic Acid (English)

FANG Xiao-Niu, LI Jia, YI Xiu-Guang, YI Zhi-Qiang, CHEN Jia-Yi, LI Yong-Xiu

DOI:10.11862/CJIC.2019.111

Chinese J. Inorg. Chem., **2019**,**35**(5):930-936



A novel copper(II) complex shows blue violet photoluminescence emission, which can be attributed to ligand-to-ligand charge transfer (LLCT), as revealed by TDDFT calculations. Solid-state diffuse reflectance measurement shows the existence of a narrow optical band gap of 1.91 eV.